IJMMM International Journal of Minerals, Metallurgy and Materials 矿物冶金与材料学报（英文版）

Enhanced electrochemical performance of Si/C electrode through surface modification using SrF_2 particle

Jun Yang, Yuan-hua Lin, Bing-shu Guo, Ming-shan Wang, Jun-chen Chen, Zhi-yuan Ma, Yun Huang, and Xing Li

Cite this article as:
Jun Yang, Yuan-hua Lin, Bing-shu Guo, Ming-shan Wang, Jun-chen Chen, Zhi-yuan Ma, Yun Huang, and Xing Li, Enhanced electrochemical performance of Si/C electrode through surface modification using SrF_2 particle, *Int. J. Miner. Metall. Mater.*, 28(2021), No. 10, pp. 1621-1628. https://doi.org/10.1007/s12613-021-2270-x

View the article online at SpringerLink or IJMMM Webpage.

International Journal of Minerals, Metallurgy and Materials
Volume 28, Number 10, October 2021, Page 1621
https://doi.org/10.1007/s12613-021-2270-x

Enhanced electrochemical performance of Si/C electrode through surface modification using SrF_2 particle

Jun Yang, Yuan-hua Lin, Bing-shu Guo, Ming-shan Wang, Jun-chen Chen, Zhi-yuan Ma, Yun Huang, and Xing Li

School of New Energy and Materials, Southwest Petroleum University, Chengdu 610500, China
(Received: 29 December 2020; revised: 2 February 2021; accepted: 24 February 2021)

Abstract: The silicon-based material exhibits a high theoretical specific capacity and is one of the best anode for the next generation of advanced lithium-ion batteries (LIBs). However, it is difficult for the silicon-based anode to form a stable solid-state interphase (SEI) during Li alloy/de-alloy process due to the large volume change (up to 300%) between silicon and $Li_{4.4}Si$, which seriously limits the cycle life of the LIBs. Herein, we use strontium fluoride (SrF_2) particle to coat the silicon−carbon (Si/C) electrode (SrF_2@Si/C) to help forming a stable and high mechanical strength SEI by spontaneously embedding the SrF_2 particle into SEI. Meanwhile the formed SEI can inhibit the volume expansion of the silicon−carbon anode during the cycle. The electrochemical test results show that the cycle performance and the ionic conductivity of the SrF_2@Si/C anode has been significantly improved. The X-ray photoelectron spectroscopy (XPS) analysis reveals that there are fewer electrolyte decomposition products formed on the surface of the SrF_2@Si/C anode. This study provides a facile approach to overcome the problems of Si/C electrode during the electrochemical cycling, which will be beneficial to the industrial application of silicon-based anode materials.

Keywords: silicon-based anode; volume expansion; strontium fluoride; solid electrolyte interface; cycling stability

1. Introduction

Since the Volta stacks have been invented more than two hundred years ago, various electrochemical energy storage devices have continuously emerged to increase the energy density of the battery systems. Up to date, lithium ion batteries (LIBs) are widely used in many different scenarios, such as portable electronics, rechargeable vehicles as well as smart power grid [1−2]. At present, the most advanced LIBs mainly use graphite carbon with stable cycle performance as the anode. However, the theoretical capacity of the graphite anode is relatively low (372 $mA{\cdot}h{\cdot}g^{-1}$) [3], which further limits the improvement of the discharge capacity and the energy density of LIBs. In contrast, silicon has a significantly higher theoretical specific capacity (4200 $mA{\cdot}h{\cdot}g^{-1}$), low working voltage (0.2−0.3 V vs. Li/Li^+), and abundant natural reserves. It is one of the best candidate anode materials for next-generation high-energy LIBs. However, the application of silicon anode is facing many challenges. Firstly, the poor electronic and ionic conductivity of silicon will lead to sluggish electron and lithium ion transmission; Secondly, the huge volume expansion (300%) during Li alloy/dealloy processes will result in pulverization of the electrode structure and further detach from the current collector; Thirdly, the uncontrollable solid-state interphase (SEI) layers caused by volume effects and initially low initial Coulombic efficiency are also the obstacles of silicon anode commercialization [4−6].

At present, great advances have been made in the exploration of silicon anode, and researchers have adopted many methods to improve the performance of it. Among them, introducing of carbon materials into silicon-based anode can effectively restrain volume expansion and enhance the electronic conductivity of the electrode. In addition, synthesis of nano-silicon materials, Such as core-shell structures [7−9], nanoparticles [10−12], nanotubes [13−14], nanowires [15−16], and nanofibers [17−19], can also mitigate the volume effect of silicon during charging and discharging. However, due to the large expansion stress of silicon during Li dealloy process, the fracture or even the shedding of the SEI from the anode surface is still inevitable, which will cause new anode surface to be exposed into the electrolyte and continue to occur side effects to form new SEI [20]. This

Corresponding authors: Yuan-hua Lin E-mail: yhlin28@163.com; Xing Li E-mail: lixing198141@yahoo.com

process will lead to irreversible consumption of electrolyte on Si/C anode material and seriously affect the cycle performance of the LIBs. Therefore, a robust and stable SEI is extremely crucial to the stability of silicon based LIBs life [20−21].

Increasing the interface energy is conducive to improving the stability of the SEI, and can promote the uniform diffusion of lithium ions, which is conducive to reducing its interface impedance [22−23]. Strontium fluoride (SrF_2) has a higher interface energy than LiF, Li_2O, Li_2CO_3, etc. It is conducive to improving the mechanical property of the SEI and can effectively inhibit the uneven deposition of lithium [24]. Previous studies have compared the effects of SrF_2, CaF_2, AlF_3, etc. on the lithium metal interface, and found that the presence of SrF_2 particles in the SEI can effectively improve the cycle stability of the lithium metal batteries. Directly coating of SrF_2 on the surface of lithium metal can also effectively inhibit the growth of lithium dendrites. The inorganic SrF_2 particles can take part in the formation of the SEI and be embedded into it, which delivers more excellent mechanical properties to the organic SEI. Thus the organic-inorganic hybrid SEI has a better stability to withstand the volume change of the lithium metal anode when it expands and contracts [25]. In this work, to further accommodate the volume effect of Si/C anode, we use the SrF_2 particle to coat the Si/C electrode to form the SEI with stronger mechanical properties. The fundamental mechanism for the SrF_2 coating to improve the electrochemical performance of Si/C anode was systematically investigated and disclosed via employing analytical techniques.

2. Experimental

2.1. Materials synthesis

The silicon−carbon (Si/C) composite material was prepared by using phenolic resin and nano-silicon powder as the precursor (phenolic : nano-silicon = 1:1 in weight ratio), which were mixed in the alcohol, stirred and evaporated to dry at 80°C. After that, the powder was dried in a vacuum oven at 80°C for 15 h. Subsequently, it was heated at 350°C for 5 h in an argon atmosphere, followed by carbonization at 700°C for 1 h to prepare the Si/C composite. The Si/C composite was employed to prepare the electrode containing Si/C active material, acetylene black, and sodium alginate binder in weight ratio of 8:1:1 (Si/C electrode). Finally, The Si/C anode was coated with a suspension of SrF_2 and polyvinylidene difluoride (PVDF) (9:1 in weight ratio) in N-methylpyrrolidone (NMP), and the coating thickness is about 15 μm (SrF_2@Si/C electrode). The SrF_2 particle was purchased from Aladdin Biochemical Technology Co., Ltd., China with a particle size of ~2 μm.

2.2. Materials characterizations

The scanning electron microscopy (SEM) with an energy dispersive X-ray spectroscopy (EDX) detector (ZEISS-EVOMA15, Germany) was used to analyze the microstructure of SrF_2 particle, the prepared Si/C and SrF_2@Si/C electrodes, and the formed solid electrolyte interphases (SEI) on the electrodes.

2.3. Electrochemical measurements

The electrochemical performances of the bare Si/C and SrF_2@Si/C electrode were tested using the CR2032 coin-type cell. The cell contains a cathode (Si/C or SrF_2@Si/C with diameter of 14 mm and active loading of 1.6 $mg \cdot cm^{-2}$) and a Li metal anode (diameter of 16 mm with the thickness of 0.6 mm). The separator is polypropylene membrane (PP) separator (Celgard 3501, diameter of 18 mm), and the electrolyte is 1 M $LiPF_6$ in ethylene carbonate (EC) : diethyl carbonate (DEC) : ethyl methyl carbonate (EMC) (1:1:1 in volume ratio) with 10wt% fluoroethylene carbonate (FEC) and 2wt% vinylene carbonate (VC) as the additives. The coin cells were assembled in a glove box with both water and oxygen contents less than 1 ppm. The assembled coin-type cells were tested using a Galvanostatic BTS-5V10mA battery tester (NEWARE Electronics Co., Ltd., China) within a voltage range of 0.01−1.5 V vs. Li/Li^+. The cyclic voltammetry (CV) and electrochemical impedance spectroscopy (EIS) was conducted using CH Instruments CHI660D. Measurement was performed for the EIS testing at the frequency ranging from 10^5 to 10^{-2} Hz, with a potential perturbation amplitude of 10 mV.

3. Results and discussion

As shown in Fig. 1(a), when the pristine Si/C composite is cycled in the Li||Si/C half-cell, its first cycle Coulombic efficiency (CE) is 77.5% and its initial discharge specific capacity is 1836 $mA \cdot h \cdot g^{-1}$ at a current rate of 300 $mA \cdot g^{-1}$. After 100 cycles, the discharge specific capacity of Li||Si/C cell decays to only 83 $mA \cdot h \cdot g^{-1}$. In contrast, the initial discharge specific capacity and the first cycle CE of Li||SrF_2@Si/C half-cell are 1549 $mA \cdot h \cdot g^{-1}$ and 76.3% at the same condition. Although the Li||SrF_2@Si/C cell shows a slightly lower initial discharge specific capacity, its discharge capacity retains at 462 $mA \cdot h \cdot g^{-1}$ after 100 cycles. Besides, Li||SrF_2@Si/C cell also displays a more stable CE after initial several cycles of activation. This indicates that during the beginning of cycles, the coated SrF_2 layer on the surface of Si/C electrode may reduce the diffusion rate or extend the diffusion path of Li^+, but after several cycles, the SrF_2 layer will gradually decrease and uniformly participate in the formation of SEI film. This process will significantly adjust the distribution of SrF_2 so that its porosity is emerged and accelerate the diffusion of Li^+. At the same time, the mechanical properties of SEI in Li||SrF_2@Si/C cell also be improved and can further buffer the volume effect of Si/C anode. Therefore, Li||SrF_2@Si/C shows a more stable cycle performance and Coulomb effi-

ciency. Figs. 1(b) and 1(c) are the charging and discharging profiles of Li||Si/C and Li||SrF_2@Si/C cells under different cycles. After 100 cycles, the discharge specific capacity of Li||Si/C is 83 mA·h·g^{-1}, whereas that of Li||SrF_2@Si/C is 462 mA·h·g^{-1}. Besides, due to limited diffusion of Li^+, the Si/C anode exhibits a lower polarization voltage than SrF_2@Si/C anode before initial several cycles. But hereafter, the polarization voltage of Si/C anode continuously increases owing to the large volume variation and brittle SEI during the charging/discharging processes.

Fig. 2 shows the CV curves of the Li||Si/C and Li||SrF_2@Si/C cells. It could be observed that the SrF_2 coating does not affect the Li^+ inserting/de-inserting processes of Si/C anode composite. Moreover, the potential differences of the redox peaks also demonstrate that the Li||SrF_2@Si/C cell shows larger polarization than Li||Si/C cell during the first 3 cycles, which should be ascribed to the SrF_2 coating layer that limits the Li^+ diffusion during the initial electrochemical cycling stage. It is also well corresponding to the first several charge and discharge profiles of Li||Si/C and Li||SrF_2@Si/C cells in Fig. 1.

Fig. 3 shows the morphologies and element characterizations of SrF_2@Si/C and Si/C anode materials. As shown in Figs. 3(d) and 3(e), the original Si/C layer on the copper (Cu) substrate shows a rough surface with a thickness of about 30 μm. After coating by SrF_2, the surface of SrF_2@Si/C anode (Fig. 3(g)) becomes flatter. Meanwhile, the Fig. 3(h) (cross section) further reveals that the thickness of SrF_2 coating layer is about 15 μm, and which also shows a good contact with Si/C electrode. Figs. 3(j) and 3(m) present the top views of Si/C and SrF_2@Si/C anodes after 100 cycles. It is worth noting that the surface of Si/C anode becomes cracked and pulverized, while the surface of SrF_2@Si/C remains flat. In addition, Fig. 3(k) shows that the thickness of the Si/C electrode becomes significantly thicker after cycling and expands from the original 30 to 65 μm. For the SrF_2@Si/C electrode, however, the thickness of the Si/C layer is relatively low (Fig. 3(n)), which is expanded from the original 45 to 65 μm (including 15 μm SrF_2 layer), indicating that the coating of SrF_2 can effectively suppress the volume change of the Si/C

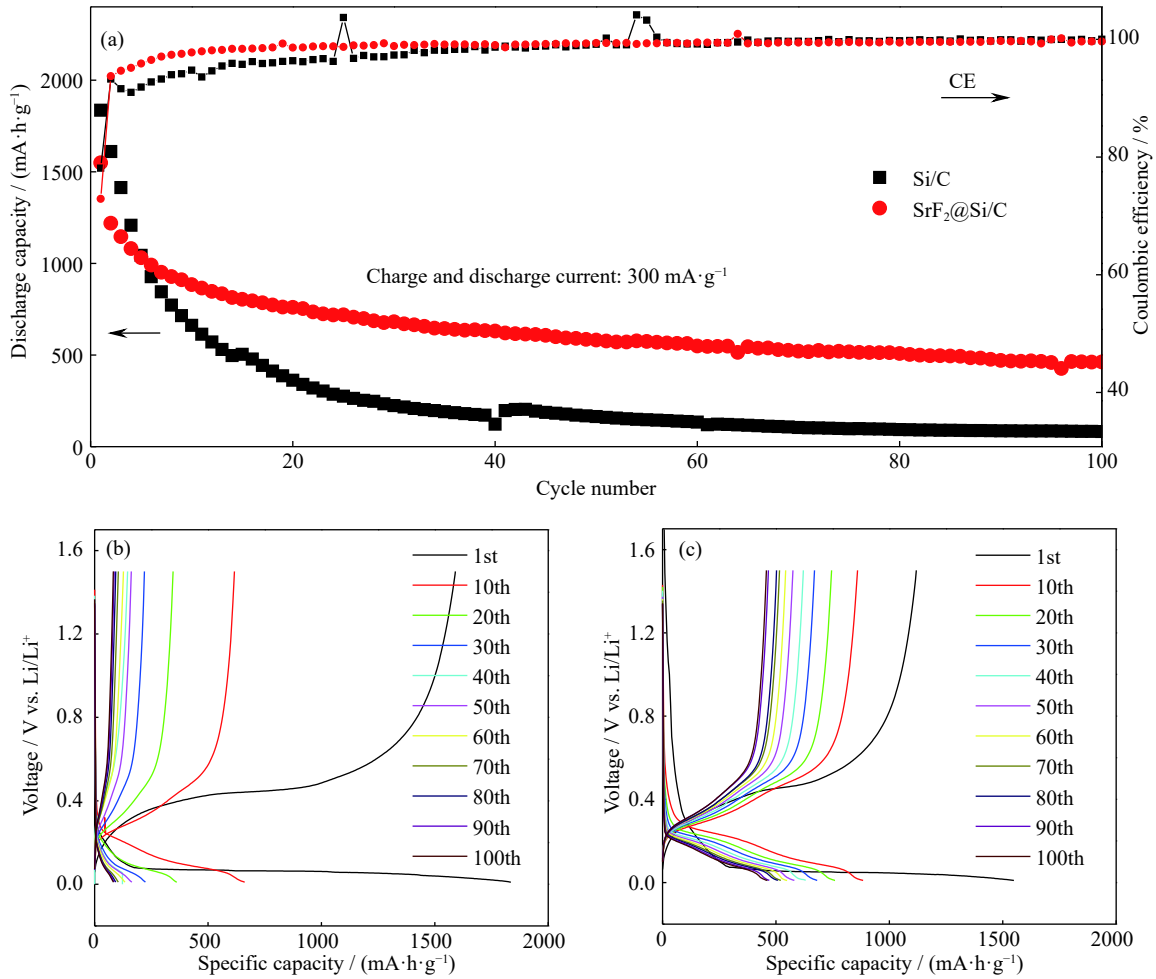

Fig. 1. Electrochemical performance tests: (a) long cycle of Li||Si/C and Li||SrF_2@Si/C cells, the voltage window and the current rate are 0.01−1.5 V and 300 mA·g^{-1}, respectively; charge and discharge profiles of (b) Li||Si/C and (c) Li||SrF_2@Si/C cells.

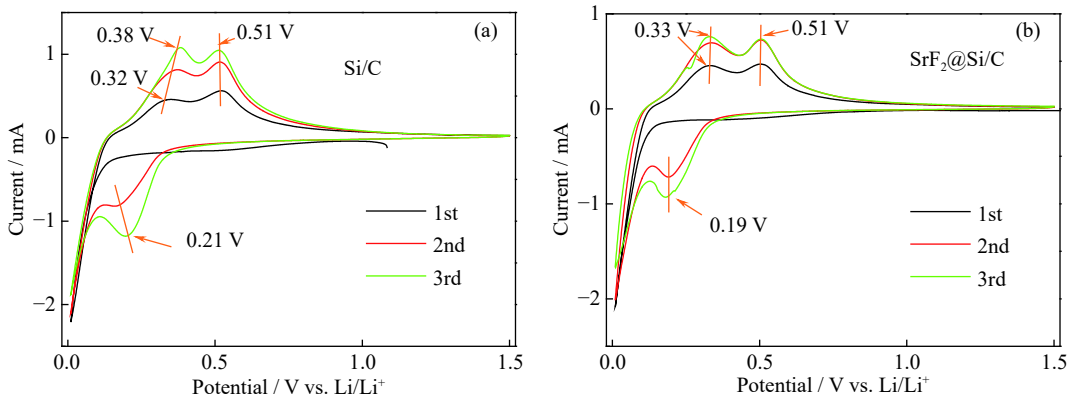

Fig. 2. CV curves of (a) Li||Si/C and (b) Li||SrF_2@Si/C cells at the cut off voltages of 0.01−1.5 V with a scanning rate of 0.1 mV/s.

anode during the electrochemical cycling. Furthermore, energy dispersive spectrometer (EDS) is employed to analyze the elemental compositions of the anode surface after cycling. From the results of EDS analysis in Figs. 3(f), 3(i), 3(l), and 3(o), a significantly smaller amount of C and O elements, which are the characteristic elements of electrolyte solvent decomposition, is detected on the surface of SrF_2@Si/C electrode than that of Si/C anode. It indicates that there is less decomposition of the electrolyte due to the protection of Si/C electrode by coating SrF_2 layer on its surface, which conduces to form a denser and more mechanically organic−inorganic hybrid SEI film. The formed robust organic-inorganic hybrid SEI film could protect the Si/C anode from being further corroded by the $LiPF_6$ based electrolyte, meanwhile the volume expansion of silicon also being well suppressed, hence enhancing the electrochemical cycling stability of Si/C anode.

We further performed the XPS analysis on the anode material after the cycle. As show in Fig. 4, the C 1s spectra show that the SEI on both of Si/C and Si/C@SrF_2 anodes all contain C−C/C−H (hydrocarbon, ~285.0 eV), C−O (polyether carbon, ~286.5 eV), and C=O/O=C−O (carbonyl group, 289.0 eV) peaks, while the O 1s spectra all consist of C=O (carbonyl, ~531.0 eV) peak. But the intensity of all peaks reveals the Si/C@SrF_2 surface has much less C−C/C−H and C=O functional groups, indicating that the electrolyte solvent on the anode surface is less degraded. This mainly benefits from the establishment of a more robust SEI, which can more effectively passivate the electrode/electrolyte interface during the volume expansion/contraction of the Si/C active material. Besides, the SiO_x (~103 eV) signal peak appears on the Si/C anode surface [26], which means that the SEI on the surface of the Si/C anode cannot effectively protect the Si/C active material. In the Sr 3d spectrum, the signals at 135.8 and 134.0 eV belong to Sr $3d_{3/2}$ and Sr $3d_{5/2}$, respectively, which are consistent well with the Sr^{2+} state rather than Sr. There is no characteristic peak of other Sr elements on the surface of Si/C@SrF_2 after the cycle, indicating that SrF_2 did not decompose during the whole cycle.

According to the previous reports, increasing the interface energy of SEI can promote a uniform flow of lithium ions to a certain extent, thereby reducing the interface impedance [22]. Therefore, the electrochemical impedance spectroscopy (EIS) was used to detect the electrochemical reaction kinetics. As shown in Fig. 5, the Nyquist plots of the Si/C and SrF_2@Si/C anodes were obtained at different cycles. Among them, the irregular semicircle in middle high frequency derives from the surface SEI film resistance (R_{SEI}) of the electrode and the charge transfer resistance (R_{CT}) between electrode and electrolyte interface [27−28]. The intercept between the semicircle and the X axis in high frequency represents the electrolyte resistance (R_e) and the low-frequency tail represents the diffusion of Li^+ in the anode material [12,29]. The oblique line in the low frequency region represents the Warburg impedance (W_0), which is related to the ion diffusion limit in the electrode. Table 1 shows the impedance fitting parameters of the anodes using the equivalent circuit as inserting in Fig. 5(a) under different cycles. For the Si/C anode (Fig. 5(a)), the R_{SEI} increases rapidly with the increase of the cycle number, but it increases slightly for the SrF_2@SiC composite material even after 100 cycles (Fig. 5(b)). The R_{SEI} values of the Si/C anode at the 10th, 50th, and 100th cycles are 2.1, 3.3, and 68.3 Ω, respectively. By comparison, the R_{SEI} values of the SrF_2@Si/C anode under the same conditions are 1.8, 2.0, and 2.0 Ω, respectively. The significantly smaller R_{SEI} of SrF_2@Si/C indicates that the SEI generated in the composite anode is more stable and conducive to the diffusion of the Li^+. In addition, the SrF_2@Si/C electrode also exhibits a significantly smaller R_{CT}. From the Figs. 3(h) and 3(n), it can be found that the SrF_2@Si/C electrode after the electrochemical cycling shows a smaller volume expansion, thereby inhibiting the destruction of the internal structure, hence resulting in smaller R_{CT} value. The R_{CT} values of the Si/C anode at the 10th, 50th, and 100th cycle are 27.6, 22.5, 75.0 Ω, respectively. By comparison, the R_{CT} values of the SrF_2@Si/C composite anode under the same conditions are 10.7, 11.3, 13.5 Ω, respectively. Figs. 5(c) and 5(d) are the relationships between $\omega^{-1/2}$ and Z' from

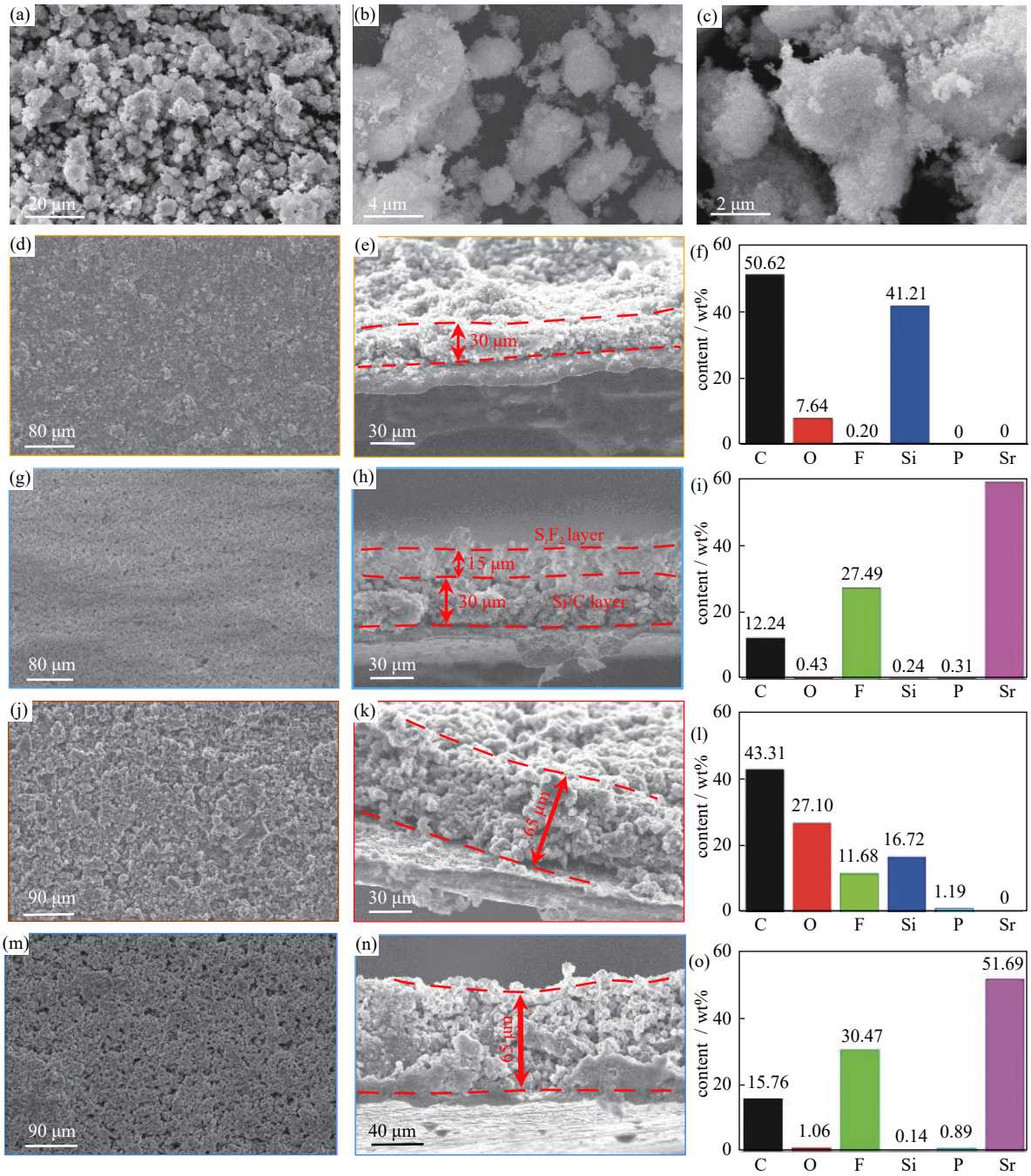

Fig. 3. SEM and EDS elements characterizations of fresh SrF_2 particle, Si/C and SrF_2@Si/C anodes: (a, b, c) fresh SrF_2 particles under different magnifications; top view, cross-section, and surface element content of fresh (d, e, f) Si/C and (g, h, i) SrF_2@Si/C anodes; top view, cross-section, and surface element content of (j, k, l) Si/C and (m, n, o) SrF_2@Si/C anodes after 100 cycles.

Si/C and SrF_2@Si/C anodes. It can be inferenced that the diffusion coefficient of Li^+ (D_{Li+}) in the Si/C anode after the 10th, 50th, and 100th cycle are 8.18×10^{-13}, 1.72×10^{-13}, and 1.48×10^{-13} $cm^{-2}\cdot s^{-1}$, while the D_{Li}^+ in SrF_2@Si/C composite anode are 9.19×10^{-12}, 1.11×10^{-12}, and 2.71×10^{-12} $cm^{-2}\cdot s^{-1}$, respectively. An order of magnitude higher D_{Li+} demonstrates that the SrF_2 coating layer can not only contribute to forming a stable SEI film and inhibiting the volume effect, but also promote the transport of Li^+ [24–25].

As shown in Fig. 6, in pure Si/C anode, due to the serious volume expansion of Si during the Li^+ alloy/de-alloy process, it is hard to form a stable SEI film on the Si/C electrode surface. Therefore, the material is easier to pulverize during the cycle and the $LiPF_6$ based electrolyte will continue to corrode the electrode surface, hence resulting in a thicker, crack, and brittle SEI. This will significantly enhance the electrode polarization and degrade the electrochemical performances. Therefore, the anode shows a looser surface after cycling and

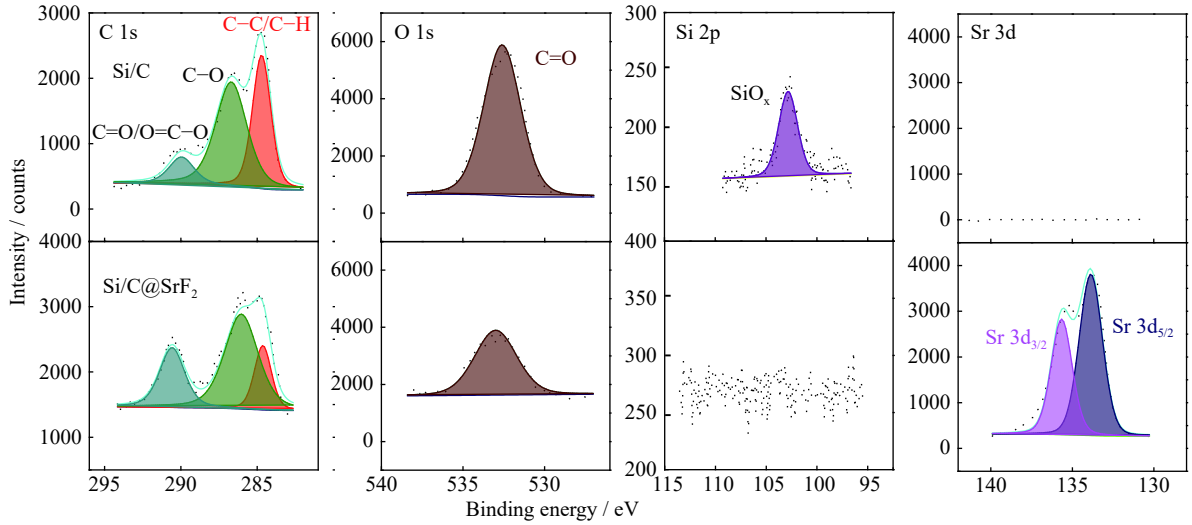

Fig. 4. C 1s, O 1s, Si 2p, and Sr 3d XPS spectra of the resulting SEI from Si/C (above) and Si/C@SrF_2 (below) anodes.

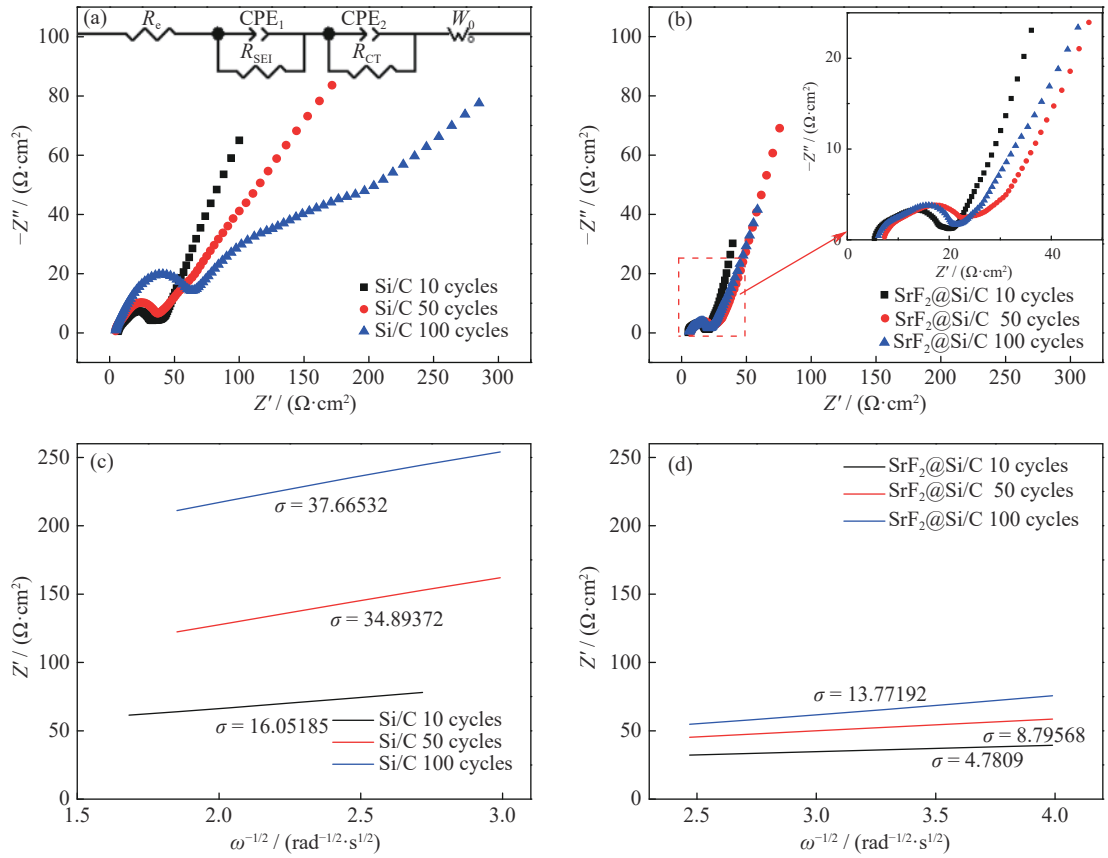

Fig. 5. Nyquist plots of (a) Li||Si/C and (b) Li||SrF_2@Si/C anodes, and data fitting of the relationships between $\omega^{-1/2}$ and Z' from (c) Si/C and (d) SrF_2@Si/C anodes (ω represents the frequency and σ represents the slope of the fitted line).

Table 1. Fitting R_e, R_{SEI}, R_{CT}, and D_{Li+} values for Li||Si/C and Li||SrF_2@Si/C cells under different cycles

Cycle number	R_e / Ω		R_{SEI} / Ω		R_{CT} / Ω		D_{Li}^+ / ($cm^{-2}·s^{-1}$)	
	Si/C	SrF_2@Si/C	Si/C	SrF_2@Si/C	Si/C	SrF_2@Si/C	Si/C	SrF_2@Si/C
10	6.1	6.0	2.1	1.8	27.6	10.7	8.18×10^{-13}	9.19×10^{-12}
50	6.3	6.2	3.3	2.0	22.5	11.3	1.72×10^{-13}	1.11×10^{-12}
100	6.3	6.1	68.3	2.0	75.0	13.5	1.48×10^{-13}	2.71×10^{-12}

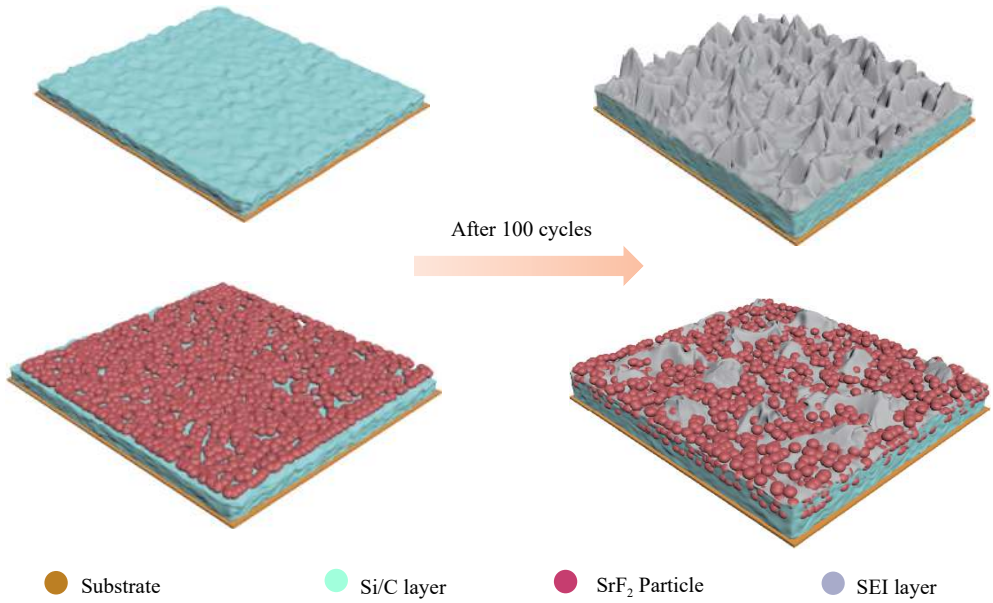

Fig. 6. Schematic diagram for the SrF_2 coating layer enhancing the electrochemical performances of Si/C anode.

relatively larger volume expansion (Fig. 3). The pulverizing Si particle will lose electrical connection with the current collector and cause a rapid capacity decrease (Fig. 1). For Si/C@SrF_2 anode, SrF_2 adheres evenly on the surface of Si/C electrode before cycling. During the cycle, SrF_2 with high electronic insulation and high interface energy will gradually participate in the formation of SEI and produce a dense and organic−inorganic hybrid SEI to strengthen the mechanical properties and the lithium ion conductivity of SEI [25]. This robust SEI can suppress the further corrosion of the electrode by the electrolyte and more adapt to the volume change of Si/C materials, thereby inhibiting the crushing of Si/C materials to a certain extent. Si/C@SrF_2 exhibits a smoother surface and smaller volume expansion after cycling. Therefore, it also reasonably explains why Si/C@SrF_2 shows better cycle performance.

4. Conclusion

In this work, we prove that coating of SrF_2 particle on the surface of Si/C anode can effectively improve its electrochemical performances. The mechanism of this process is attributed to the fact that SrF_2 can help to form a SEI with better mechanical, dense, and ion conductive properties, which can also effectively prevent the Si/C material from pulverizing and falling off from the conductive substrate due to the volume expansion during the electrochemical cycling. Actually, this work provides a simple and dependable strategy to form an effective SEI on silicon-based anode electrode to overcome the problems of the volume expansion, active material particle pulverizing, peeling off, electrode polarization, etc., which would provide some guidance for the industrial application of silicon-based anodes.

Acknowledgements

This work was financially supported by the National Natural Science Foundation of China (No. 52072322) and the Department of Science and Technology of Sichuan Province, China (Nos. 2019YFG0220 and 2019-GH02-00052-HZ).

References

[1] J.B. Goodenough and K.S. Park, The Li-ion rechargeable battery: A perspective, *J. Am. Chem. Soc.*, 135(2013), No. 4, p. 1167.

[2] L.F. Wang, M.M. Geng, X.N. Ding, C. Fang, Y. Zhang, S.S. Shi, Y. Zheng, K. Yang, C. Zhan, and X.D. Wang, Research progress of the electrochemical impedance technique applied to the high-capacity lithium-ion battery, *Int. J. Miner. Metall. Mater.*, 28(2021), No. 4, pp. 538-552.

[3] M. Winter, B. Barnett, and K. Xu, Before Li ion batteries, *Chem. Rev.*, 118(2018), No. 23, p. 11433.

[4] Y. Jin, B. Zhu, Z.D. Lu, N. Liu, and J. Zhu, Challenges and recent progress in the development of Si anodes for lithium-ion battery, *Adv. Energy Mater.*, 7(2017), No. 23, p. 1700715.

[5] A. Iqbal, L. Chen, Y. Chen, Y. X. Gao, F. Chen, and D.C. Li, Lithium-ion full cell with high energy density using nickel-rich $LiNi_{0.8}Co_{0.1}Mn_{0.1}O_2$ cathode and SiO−C composite anode, *Int. J. Miner. Metall. Mater.*, 25(2018), No. 12, p. 1473.

[6] H. Wu and Y. Cui, Designing nanostructured Si anodes for high energy lithium ion batteries, *Nano Today*, 7(2012), No. 5, p. 414.

[7] L.F. Cui, R. Ruffo, C.K. Chan, H.L. Peng, and Y. Cui, Crystalline-amorphous core-shell silicon nanowires for high capacity and high current battery electrodes, *Nano Lett.*, 9(2009), No. 1, p. 491.

[8] W. Wang, Y.W. Wang, L. Gu, R. Lu, H.L. Qian, X.S. Peng, and J. Sha, SiC@Si core-shell nanowires on carbon paper as a hybrid anode for lithium-ion batteries, *J. Power Sources*, 293(2015), p. 492.

[9] Y.W. Hu, X.S. Liu, X.P. Zhang, N. Wan, D. Pan, X.J. Li, Y. Bai, and W.F. Zhang, Bead-curtain shaped SiC@SiO_2 core-shell nanowires with superior electrochemical properties for lithium-ion batteries, *Electrochim. Acta*, 190(2016), p. 33.

[10] U. Kasavajjula, C.S. Wang, and A.J. Appleby, Nano- and bulk-silicon-based insertion anodes for lithium-ion secondary cells, *J. Power Sources*, 163(2007), No. 2, p. 1003.

[11] A. Magasinski, P. Dixon, B. Hertzberg, A. Kvit, J. Ayala, and G. Yushin, High-performance lithium-ion anodes using a hierarchical bottom-up approach, *Nat. Mater.*, 9(2010), No. 4, p. 353.

[12] X. Li, Y.S. Bai, M.S. Wang, G.L. Wang, Y. Ma, L. Li, B.S. Xiao, and J.M. Zheng, Self-assembly encapsulation of Si in N-doped reduced graphene oxide for use as a lithium ion battery anode with significantly enhanced electrochemical performance, *Sustainable Energy Fuels*, 3(2019), No. 6, p. 1427.

[13] M.H. Park, M.G. Kim, J. Joo, K. Kim, J. Kim, S. Ahn, Y. Cui, and J. Cho, Silicon nanotube battery anodes, *Nano Lett.*, 9(2009), No. 11, p. 3844.

[14] Y. Zhang, K. Hu, Y.L. Zhou, Y.B. Xia, N.F. Yu, G.L. Wu, Y.S. Zhu, Y.P. Wu, and H.B. Huang, A facile, one-step synthesis of silicon/silicon carbide/carbon nanotube nanocomposite as a cycling-stable anode for lithium ion batteries, *Nanomaterials*, 9(2019), No. 11, p. 1624.

[15] C.K. Chan, H.L. Peng, G. Liu, K. McIlwrath, X.F. Zhang, R.A. Huggins, and Y. Cui, High-performance lithium battery anodes using silicon nanowires, *Nat. Nanotechnol.*, 3(2008), No. 1, p. 31.

[16] K.Q. Peng, J.S. Jie, W.J. Zhang, and S.T. Lee, Silicon nanowires for rechargeable lithium-ion battery anodes, *Appl. Phys. Lett.*, 93(2008), No. 3, p. 033105.

[17] H.W. Mi, F. Li, S.X. Xu, Z.A. Li, X.Y. Chai, C.X. He, Y.L. Li, and J.H. Liu, A tremella-like nanostructure of silicon@void@graphene-like nanosheets composite as an anode for lithium-ion batteries, *Nanoscale Res. Lett.*, 11(2016), No. 1, p. 204.

[18] B. Wang, X.L. Li, B. Luo, Y.Y. Jia, and L.J. Zhi, One-dimensional/two-dimensional hybridization for self-supported binder-free silicon-based lithium ion battery anodes, *Nanoscale*, 5(2013), No. 4, p. 1470.

[19] M.S. Wang, W.L. Song, and L.Z. Fan, Three-dimensional interconnected network of graphene-wrapped silicon/carbon nanofiber hybrids for binder-free anodes in lithium-ion batteries, *ChemElectroChem*, 2(2015), No. 11, p. 1699.

[20] H.P. Jia, L.F. Zou, P.Y. Gao, X. Cao, W.G. Zhao, Y. He, M.H. Engelhard, S.D. Burton, H. Wang, X.D. Ren, Q.Y. Li, R. Yi, X. Zhang, C.M. Wang, Z.J. Xu, X.L. Li, J.G. Zhang, and W. Xu, High-performance silicon anodes enabled by nonflammable localized high-concentration electrolytes, *Adv. Energy Mater.*, 9(2019), No. 31, p. 1900784.

[21] S. Chattopadhyay, A.L. Lipson, H.J. Karmel, J.D. Emery, T.T. Fister, P.A. Fenter, M.C. Hersam, and M.J. Bedzyk, *In situ* X-ray study of the solid electrolyte interphase (SEI) formation on graphene as a model Li-ion battery anode, *Chem. Mater.*, 24(2012), No. 15, p. 3038.

[22] Y.Y. Lu, Z.Y. Tu, and L.A. Archer, Stable lithium electrodeposition in liquid and nanoporous solid electrolytes, *Nat. Mater.*, 13(2014), No. 10, p. 961.

[23] H. Jia, L. Zou, P. Gao, X. Cao, W. Zhao, Y. He, M.H. Engelhard, S.D. Burton, H. Wang, X. Ren, Q. Li, R. Yi, X. Zhang, C. Wang, Z. Xu, X. Li, J. G. Zhang, and W. Xu, High-performance silicon anodes enabled by nonflammable localized high-concentration electrolytes, *Adv. Energy Mater.*, 9(2019), art. No.1900784.

[24] S.F. Liu, X. Ji, J. Yue, S. Hou, P.F. Wang, C.Y. Cui, J. Chen, B.W. Shao, J.R. Li, F.D. Han, J.P. Tu, and C.S. Wang, High interfacial-energy interphase promoting safe lithium metal batteries, *J. Am. Chem. Soc.*, 142(2020), No. 5, p. 2438.

[25] X. Li, Y. Liu, Y. Pan, M.S. Wang, J.C. Chen, H. Xu, Y. Huang, W.M. Lau, A.X. Shan, J.M. Zheng, and D. Mitlin, A functional SrF_2 coated separator enabling a robust and dendrite-free solid electrolyte interphase on a lithium metal anode, *J. Mater. Chem. A*, 7(2019), No. 37, p. 21349.

[26] C.C. Nguyen, T. Yoon, D.M. Seo, P. Guduru, and B.L. Lucht, Systematic investigation of binders for silicon anodes: Interactions of binder with silicon particles and electrolytes and effects of binders on solid electrolyte interphase formation, *ACS Appl. Mater. Interfaces*, 8(2016), No. 19, p. 12211.

[27] X. Li, K.J. Zhang, D. Mitlin, E. Paek, M.S. Wang, F. Jiang, Y. Huang, Z.Z. Yang, Y. Gong, L. Gu, W.G. Zhao, Y.G. Du, and J.M. Zheng, Li-rich $Li[Li_{1/6}Fe_{1/6}Ni_{1/6}Mn_{1/2}]O_2$ (LFNMO) cathodes: Atomic scale insight on the mechanisms of cycling decay and of the improvement due to cobalt phosphate surface modification, *Small*, 14(2018), No. 40, p. 1802570.

[28] X. Li, K.J. Zhang, D. Mitlin, Z.Z. Yang, M.S. Wang, Y. Tang, F. Jiang, Y.G. Du, and J.M. Zheng, Fundamental insight into Zr modification of Li- and Mn-rich cathodes: Combined transmission electron microscopy and electrochemical impedance spectroscopy study, *Chem. Mater.*, 30(2018), No. 8, p. 2566.

[29] X. Li, Y.S. Bai, M.S. Wang, G.L. Wang, Y. Ma, Y. Huang, and J.M. Zheng, Dual carbonaceous materials synergetic protection silicon as a high-performance free-standing anode for lithium-ion battery, *Nanomater.*, 9(2019), No. 4, p. 650.